Idle active matter: excavation by confined and crowded collectives

D. Monaenkova[1]*, J. Aguilar[2]*, V. Linevich[2], W. Savoie[1], B. Dutta[1], M. A. D. Goodisman[3], D. I. Goldman[1]*.

[1] School of Physics, Georgia Institute of Technology, Atlanta, GA, USA

[2]School of Mechanical Engineering, Georgia Institute of Technology, Atlanta, GA, USA

[3]School of Biological Sciences, Georgia Institute of Technology, Atlanta, GA, USA

*Correspondence to: daniel.goldman@physics.gatech.edu

†Additional author notes should be indicated with symbols (for example, for current addresses).

Abstract (100-150): Ensembles of self-propelling elements can spontaneously form clusters, clogs and jams. In some active materials, avoiding structure formation is important for task completion, for example, during nest formation by social insects. We studied biological and mechanical collectives, including fire ant colonies, cellular automata models, and autonomous robots, to demonstrate the importance of appropriate individual and group-wide behaviors in facilitating tasks by crowded, confined active matter. We used tools from the study of glasses and dense particulate ensembles to provide insight into mechanisms by which congestion, jams and even arrest due to high-density traffic can be mitigated via group-level behaviors, such as idleness, as well as local interactions, such as selective retreats. combination of these strategies are used by the ants and robustly emerge from optimization algorithms, enabling the largely idle active matter to perform a task without sophisticated sensing, planning and global control of the collective.

One Sentence Summary (150): Experiments and simulations of biological and mechanical collectives reveal how workforce heterogeneity governs the successful organization of confined collectives.

Ensembles of self-propelling elements, such as active materials (*1, 2*), swarms (*3, 4*) and flocks (*5*), are of interest in many communities. Much attention has been paid to "bottom-up" study of how different rules among elements lead to collective behaviors like aggregations, schools, and collective whirls. However, less is known about how to design effective collective behaviors from the "top-down". That is, directing an active material to perform tasks, which we define as behaviors of the collective with clear control goals, remains a challenge, particularly in complex environments.

It is relatively straightforward to design a behavior that requires a collective to form an aggregation. In fact, a diversity of artificial and living active materials *spontaneously* form patterns and structures including colloidal surfers (*6*), organismal collectives (*3*), robot swarms (*7*) and theoretical models (*1, 2, 8*). In many open or unconfined biological systems (e.g. fish schools (*9*) or bird flocks (*5*)), such large scale ordering has beneficial biological functions (*10, 11*). For example, schooling behavior in fish is associated with defense against predators and foraging success. And robotic systems can benefit from aggregations in situations like self-assembly and foraging (*4*).

It is less clear how to design a system to prevent aggregations and structures from forming, which is important in tasks that demand steady flow and limited clogs, particularly in the absence of global knowledge of the state of all elements. This is particularly relevant in high density confined active systems where flow is critical and clogs tend to readily form glass-like arrests of flow; such clogs occur, for example in pedestrian/vehicular traffic jams (*12*), competing bacteria biofilms (*13*), high density cell migration (*14*), jammed herds (*15*), and robot swarms (see (*7, 16, 17*) (*18*) and *Fig. 1C, Fig. 4, supplementary materials*). While robotics has made progress in such systems as centrally controlled (assuming full knowledge of all components of active material) swarms, or allocating tasks through local response (e.g. a robot making a decision based on its local environment), these strategies are rarely tested in robophysical experiments in realistic conditions (*4*) such as confined environments.

Collective nest excavation is an example of a task that demands smooth flow of active matter without central control. Subterranean insect colonies (*19*) like fire ants (*S. invicta*) rapidly create complex networks of narrow tunnels from soil (*Fig. 1A*) (*20*) while bi-directionally trafficking the confined spaces therein. We have shown that their excavation mechanics are stereotyped, aiding the mechanics of movement and construction (*21*). Moreover, certain behaviors are important for traffic flow. We used tools from soft matter physics to show that fire ants maintain smooth flow by minimizing their interaction times (*22*); such interactions could be thought of as preventing glass-like arrest in the system.

We study nest excavation of *S. invicta* to understand how social behaviors improve performance, through either reactive mechanisms that adapt to traffic or proactive measures that avoid traffic disruptions (*Fig. 1B*). Our central hypothesis is that the advanced collective behavior seen in these ants is related to the need to flexibly perform tasks in complex environments, such that task completion remains robust to leadership and member loss, and does not require central command and control. Further, we argue that purely local rules among elements will not suffice. Instead, we envision that active materials and swarms will require group-level interactions through "sociality" — defined as cooperation strategies among individuals — promoting a flowing, non-glassy state.

Ant experiments: Small groups (~30) of *S. invicta* workers were placed in transparent containers of wetted 0.25 mm diameter glass particles (*Fig. 2A*) with a soil moisture content, defined as the ratio of total water weight to total solid weight, of W=0.01 or 0.1 (3 trials each) (*23*). Ants excavated for 48 hours (with a single ant entering the tunnel up to 426 times) and used a variety of techniques to collect grains, form pellets, and ascend the tunnel for deposition (*23*). A camera mounted to a motorized linear stage tracked a region within ~3 body-lengths from the tunnel face it was excavated (*Fig. 2A, supplementary materials*). We distinguished individual ant activity by marking ant abdomens with different colors (*Fig. 1B*). The presence and behavior of each worker that entered the tunnel was logged when in the camera's view (*Fig. 2C*).

Ants exhibited a variety of behaviors during the collective excavation bouts. A large fraction (22 ± 10% for W=0.01 soil moisture and 31 ± 13% for W=0.1) of ants never entered the tunnel to excavate during the 48-hour period of observation; we refer to these as "non-visitors". As clear in Fig 2C, there was a diversity in activity of ants that visited the tunnel face; we refer to these as "visiting" ants. Inspired by work in honeybees (*24*), we calculated the Lorenz curves (*Fig. 2D*) to illustrate activity inequality among visitor ants; these concave curves link the cumulative share of

workers in the population to the cumulative share of activity by the group. We note that about 20% of visitor ants trips did not result in extraction of a pellet (see *Movie S1* and discussion below); we included these "reversals" in the Lorenz curve calculations since these animals expended energy in a trip to the tunnel face and contributed to tunnel traffic.

To describe the Lorenz curve distributions, following (*24*), we calculated the Gini coefficient G -- the ratio of the area between the Lorenz curve and the line of equality to the area under the line of equality. G is a measure of the deviation of the workload from either perfectly shared (G = 0, all workers work equally) to completely unequal (G = 1, a single worker performs all work). Lorenz curves were characterized by G = 0.59 ± 0.07 and displayed similar functional forms across a variety of experimental conditions (see *Fig. S2*). Workload inequality has been observed in other social animals during foraging (*24*) and may change depending on the colony needs (*25*).

To investigate temporal variation in ant excavation behaviors, we divided the experiments into 12-hour "epochs". Within the first 12 hours, the workload distribution was similar to the 48-hours distribution (G = 0.52 ± 0.08 regardless of soil moisture content, p=0.39). While the activity level of individual ants changed over time (*Fig. S3*), the collective workload inequality remained consistent (*Fig. S1*) though with a slight decrease in the Gini coefficient across epoch (1-way ANOVA, $F_{2, 20} = 0.83$, $p = 0.02$). Furthermore, when the most active excavators were removed from the group, other workers increased their activity and compensated for the loss, preserving the shape of the Lorenz curve and producing similar values of the Gini coefficient (1-way ANOVA, $F_{1, 4} = 2.47$, $p = 0.2$) (*Fig. 2D inset, supplementary materials*). Thus, given the consistency of the workload distribution, we hypothesize that variations in idleness within a population may play an adaptive role in modulating the crowded conditions of confined tunnels.

The reversal behaviors (26±13% of trips for W=0.01 soil moisture and 18±3% for W=0.1, both noted for first three hours) were often associated with local crowding (*Fig. 2E*) at the excavation face (16 ± 12% of trips in W=0.01 soil moisture and 10 ± 2% of observations in W=0.1 over the first three hours). Reversal behavior in crowded conditions occurs on foraging trails (*26*), and similar phenomena have been observed in swarming bacteria (*27*). The frequency of this seemingly unproductive behavior increased with increasing overall activity of ants (*Fig. S4*). We posit that such behavior serves as a feedback mechanism for controlling congestion during excavation.

Ant simulations: To systematically examine the effects of group-level idleness and individual retreating behaviors, we developed a cellular automata (CA) excavation model (*Fig. 3A, supplementary materials*); such models have proven useful to elucidate the dynamics of ant traffic (*22, 28*). The model consisted of a lattice (the "tunnel") with a width of two cells occupied by soil, empty space, an ascending CA "ant", or a descending CA ant (*Fig. 3A*). The CA ants could move, excavate, deposit a pellet, or rest. We implemented reversals and unequal workload distributions on populations of 2 to 100 CA ants. Reversals occurred with a certain probability (*supplementary materials)* when a CA ant's desired destination was occupied and its current direction was towards the tunnel face. While direct control of output workload distributions was not implemented, we modulated workload inequality by setting individual "work probabilities" defined as the probability a CA ant would return to the excavation site after pellet deposition.

The collective work probability distribution (the "workload distribution") was determined with a

genetic algorithm (GA) (*Fig. 3B*) for a 30-ant CA model. The GA functioned by modifying individual ants work probability distribution to optimize excavation rate with each generation (*supplementary materials*). Regardless of the initial population parameters, the GA simulation converged to an unequal workload distribution within a few generations (*Fig. 3C*). Activity for the workload distribution was measured by counting instances when ants visited the tunnel within 3 body lengths (cells) of the excavation site (emulating how the camera tracks the tunnel face in the biological experiments). Notably, this optimized distribution resembled the experimentally observed biological workload distributions (*Fig. 2D, green*), suggesting that an unequal workload distribution is a robust mechanism and biological adaptation for improving excavation rate. We hypothesize that selective pressure on colonies for digging efficacy may lead to an embedded idleness in populations of underground excavators. Thus, individual worker idleness would represent a kin-selected adaptation permitting for the success of collectives.

Populations greater than three CA ants resulted in irresolvable clogs, regardless of the workload distribution, unless CA ants were capable of reversal behaviors. Thus, we simulated the behavior of CA ants using both equal workload distribution (which we refer to as "Active" CA ants) and optimized workload distribution (which we refer to as "Lorenz" CA ants) with identical reversal probabilities (*Movie S3*). Simulation parameters were selected such that 30 Lorenz CA ants reproduced experimentally observed biological ant digging rates (*Fig. 2B*).

Even with reversal behaviors, Active CA ants performed poorly for populations greater than five, whereas Lorenz CA ants maintained relatively high excavation rates even with large populations (*Fig. 3D*). Our simulations further revealed that implementation of a Lorenz workload distribution along with reversal behaviors yielded excavation benefits whereas the Active distribution performed poorly for even modest numbers of ants. Degradation of system performance when individuals attempt to maximize their own performance is common for various multi-agent systems including bridge-building army ants (*29*) and vehicle traffic (*30*). Notably, the flow in our CA models resembles characteristics of vehicle traffic flow (*31*), whereby the mean flow rate ($\bar{q}$, in our case, defined as the rate of successfully depositing ants over time) of excavators in the tunnel is maximal at an intermediate tunnel density ($\bar{\rho}$, ratio of average number of ants in the tunnel to tunnel size) (*Fig. 3E*). This trend in $\bar{q}$ vs $\bar{\rho}$ (the fundamental diagram) has been attributed to the transition between steady flow and propagating traffic jams as density increases (*32*). Thus, we attribute the increased flow rate in higher populations of Lorenz ants to a reduction in overall tunnel densities afforded by an unequal workload distribution, thereby reducing the frequency of traffic jams for large ant populations.

Robophysics experiments: CA simulations provide some insight into how various social behaviors affect excavation efficacy. However, simple simulations cannot *a priori* account for how real world complexities such as friction, agent geometry, maneuverability, and the nonexistence of traffic lanes affect system dynamics. Thus, we developed an experimental system of excavating robophysical models (*Fig. S10*) to systematically explore the various strategies above (*Fig. 4A-D*).

Teams of robots were tasked with excavating a model cohesive granular medium, hollow plastic spheres containing loose magnets. We constructed a tunnel with a width of 3 robot widths (or 1.5 robot lengths), emulating the challenge of turning around in confined spaces. We attempted to model robot behaviors on those used by biological systems (*Movie S3*). For example, rather than

using centralized control, intelligent planning, or communication, ants navigated confined spaces with local cues like head-on contact and pheromone feedback (*26*). Similarly, our robots followed simple movement instructions triggered by onboard sensory feedback of the surrounding environment (*supplementary materials*). Previous work in swarming (*33*) used similar bioinspired decentralized strategies in conjunction with collision avoidance schemes (*4*) to produce emergent flocking behavior. In contrast, our robots detected collisions with push switches on their outer shell, which triggered navigation strategies such as steering away and reversing to promote emergent clog resolution (*Movie S4*). However, in our confined system, we hypothesize that smooth traffic flow is achieved not only through reactive local strategies like reversals, but also through a group-level coordination of task distribution.

The effects of reversals and idleness distributions on robot group performance were examined individually for the three behavioral strategies described above (*Movie S5*). The first strategy (Active, *Fig. S7*) assigned equal maximal attempted activity to all diggers: after soil deposition, each robot immediately returned to the tunnel to excavate. In the second protocol (Reversal, *Fig. S8*) the robots were also programmed to immediately resume excavation after deposition but were additionally given a reversal probability. In the third protocol (Lorenz, *Fig. S9*), we implemented an unequal probability to excavate derived from experimental ant workload inequalities.

We analyzed the global traffic dynamics of the robots in the main tunnel area (i.e. excluding the excavation site) using position tracking (*supplementary material*, *Fig. S11*, see *Fig. 4B-D* for sample space-time overlap maps of robot positions). The traffic flow of robotic ants was similar to that obtained in the CA model and sensitive to the tunnel density, ρ_T (N_T/L_T, where N_T is the average number of robots in the main tunnel area), maximal at an intermediate ρ_T, followed by a gradual decline at higher ρ_T (*Fig. S12 A*).

We found that each digging strategy produced distinct trends in tunnel density and energy expenditure (*Fig. S12 B*). The Reversal strategy exhibited peak excavation performance with two robots, and monotonically increasing density and energy cost for trials with more diggers. The Lorenz strategy consistently resulted in low tunnel density and energy cost. Whereas the Active strategy resulted in a dramatic decrease in density and increase in energy expenditure with addition of a fourth robot. Therefore, strategies that minimized individual work effort sometimes led to maximized overall digging success. Dynamically allocating tasks through local feedback (*34*) or even controlling for equal workload (*35*) have proven effective in achieving robotic swarming goals such as foraging and construction. However, we find that a predefined unequal workload distribution is crucial for clog reduction in confined scenarios.

To understand these global traffic dynamics, we examined the dynamics of local robot aggregations, defined as clusters of robots within a robot length's proximity of each other, at each video frame. Multi-robot aggregations were common among all strategies and particularly frequent at the excavation site (histograms in *Fig. 4B-D*). Such clusters produced a phase separation (*8*) in the system, whereby a portion of robots were jammed at high density, while others moved smoothly through the tunnel at low density. To understand how clusters dissolved at the excavation site, we measured the mobility of each aggregation with a density overlap correlation function, $Q(\tau)$. This technique has been applied to the analysis of ant traffic (*22*), but is more traditionally used to examine dynamic heterogeneities in non-active matter such as soft

matter systems (*36*). The metric Q(τ), derived here from image correlation algorithms used in PIV (*37*) (*Fig. 4G inset*, *Fig. S13*, *supplementary materials*), compares the spatial overlap of an aggregation at a specific time to the overlap of the aggregation's original lateral segment at a later time, τ. We calculated the relaxation time, τ*, of aggregations of a specific number of diggers, N, by fitting a stretched exponential function, $Q_f(\tau) = e^{\left\{-\left(\frac{\tau}{\tau^*}\right)^{\beta}\right\}}$, to a Q curve averaged over aggregations of the same N. For 3-robot trials, all strategies produced relatively low τ* regardless of N (*Fig. 4F*). However, the addition of a fourth robot dramatically changed the relative dynamics of the three strategies.

The Active strategy revealed how aggregation dissolution was sensitive to the confinement caused by the tunnel. In particular, larger N jams resulted in increasingly higher τ*. Thus, 2-robot aggregations led to 3-robot aggregations, which consequently led to catastrophic 4-robot jams that spanned the tunnel width. Such jams were difficult to resolve with the robots' limited library of maneuvers. Unlike ants, which can climb over each other and self-deform, the robots were limited to turning and reversing maneuvers, leading to collisions that were exacerbated by the robots' rigid oblique shape (*Fig. 4E*).

Surprisingly, given their similar performance, different mechanisms emerged in the Reversal and Lorenz strategies for mitigating catastrophic jamming. Due to the robots ceasing excavation and returning to the tunnel exit after some time in a jam, the Reversal strategy established an upper limit on τ*, breaking the cascading chain-reaction effect observed in Active trials. The unequal workload distribution of the Lorenz strategy also avoided 4-robot aggregations, resulting in similarly low τ* as 3-robot trials. An analysis of relaxation times for clusters with similar aggregation density, ρ (N/L), during 4-robot experiments (*Fig. 4H*) revealed a sharp increase in τ* for the Active strategy past a local density of 1, reminiscent of glassy arrest in particulate systems (*38*). The Reversal strategy did not exhibit this glass-forming characteristic. While the Lorenz strategy occasionally exhibited glass-like catastrophic jams at higher densities, examination of the distribution of aggregation frequency vs ρ (*Fig. 4G*) revealed how the Lorenz strategy largely avoided these high densities. In particular, robot inactivity under the Lorenz strategy resulted in overall increased efficiency of the collective. We posit that task-oriented active matter systems at high density must utilize similar social strategies to mitigate catastrophic long-time flow disruption.

Our biological experiments in concert with cellular automata simulations and robophysical experiments reveal how task-oriented active matter can benefit from sociality, here in the form of novel workload distributions (e.g. majority idleness), as well as simple local rules (e.g. reversal behaviors of individuals). Such strategies can lead to emergent regulation of density in the tunnel, mitigating potentially deleterious clustering. We hypothesize that development of such collective behaviors is crucial to flow stabilization in biological task-oriented systems, and particularly to the evolution of confined social colonies (*39*). From an engineering perspective, we posit that swarming robots can benefit from such control schemes when confronted with communication and locomotor limitations and challenges. Even in the absence of complex protocols and sophisticated modes of locomotion, these strategies allow engineers to modulate swarming confined traffic. As such, the control templates discovered here may aid in tasks like smooth caravans and carpools in autonomous vehicles, debris excavation, mapping of complex

terrain as well as lunar and asteroid mining (*17*). Finally, we note that in addition to the fascinating hydrodynamic (*1*, *2*) aspects of active matter, concepts and tools developed in the soft matter physics community (e.g. in the study of supercooled fluids, granular materials and glasses) can aid in behavior design and analysis when these systems become crowded and confined.

Acknowledgements: The authors acknowledge the support of National Science Foundation grants number NSF PoLS-0957659, PHY-1205878 as well as ARO W911NF-13-1-0347 and The National Academies Keck Futures Initiative. The authors thank to Wayne Gardener, Griffin Botanical Garden and Chattahoochee-Oconee National Forest for giving us permission for ant collection. We would also like to acknowledge Dr. Nick Gravish for insight and fruitful discussions, and Dr. Mark Kingsbury and Lillian Chen for assistance in magnetic particle construction, Rachel Kutner, Romik Srivatsava, Julia Logan for their help with video analysis, and Nathaniel Conn with ant collection.

References:

1. S. Ramaswamy, in *Annual Review of Condensed Matter Physics, Vol 1*, J. S. Langer, Ed. (Annual Reviews, Palo Alto, 2010), vol. 1, pp. 323-345.
2. M. Marchetti *et al.*, Hydrodynamics of soft active matter. *Reviews of Modern Physics* **85**, 1143 (2013).
3. A. Okubo, Dynamical aspects of animal grouping: Swarms, schools, flocks, and herds. *Advances in Biophysics* **22**, 1-94 (1986).
4. M. Brambilla, E. Ferrante, M. Birattari, M. Dorigo, Swarm robotics: a review from the swarm engineering perspective. *Swarm Intelligence* **7**, 1-41 (2013).
5. W. Bialek *et al.*, Statistical mechanics for natural flocks of birds. *Proceedings of the National Academy of Sciences* **109**, 4786-4791 (2012).
6. J. Palacci, S. Sacanna, A. P. Steinberg, D. J. Pine, P. M. Chaikin, Living Crystals of Light-Activated Colloidal Surfers. *Science* **339**, 936-940 (2013).
7. L. Giomi, N. Hawley-Weld, L. Mahadevan, in *Proc. R. Soc. A.* (The Royal Society, 2013), vol. 469, pp. 20120637.
8. G. S. Redner, M. F. Hagan, A. Baskaran, Structure and dynamics of a phase-separating active colloidal fluid. *Physical review letters* **110**, 055701 (2013).
9. Y. Katz, K. Tunstrom, C. C. Ioannou, C. Huepe, I. D. Couzin, Inferring the structure and dynamics of interactions in schooling fish. *Proceedings of the National Academy of Sciences of the United States of America* **108**, 18720-18725 (2011).
10. A. Cavagna *et al.*, Scale-free correlations in starling flocks. *Proceedings of the National Academy of Sciences* **107**, 11865-11870 (2010).
11. M. Ballerini *et al.*, Interaction ruling animal collective behavior depends on topological rather than metric distance: Evidence from a field study. *Proceedings of the National Academy of Sciences* **105**, 1232-1237 (2008).
12. D. Helbing, Traffic and related self-driven many-particle systems. *Reviews of Modern Physics* **73**, 1067-1141 (2001).
13. N. C. Darnton, L. Turner, S. Rojevsky, H. C. Berg, Dynamics of Bacterial Swarming. *Biophysical Journal* **98**, 2082-2090 (2010).
14. E. Méhes, T. Vicsek, Collective motion of cells: from experiments to models. *Integr. Biol.* **6**, 831-854 (2014).
15. A. Garcimartín *et al.*, Flow and clogging of a sheep herd passing through a bottleneck. *Physical Review E* **91**, (2015).
16. L. G.-B. Yash Mulgaonkar, Anurag Makineni, and Vijay Kumar, Bio-inspired Swarms of Small Aerial Robots (submitted). *Interface Focus*, (2017).

17. P. T. Metzger, Space development and space science together, an historic opportunity. *Space Policy* **37**, 77-91 (2016).
18. V. Linevich, D. Monaenkova, D. I. Goldman, Robophysical study of excavation in confined environments. *Artificial Life and Robotics* **21**, 460-465 (2016).
19. D. M. Gordon, The organization of work in social insect colonies. *Nature* **380**, 121 (1996).
20. D. Cassill, W. R. Tschinkel, S. B. Vinson, Nest complexity, group size and brood rearing in the fire ant, Solenopsis invicta. *Insectes Sociaux* **49**, 158-163 (2002).
21. N. Gravish, D. Monaenkova, M. A. Goodisman, D. I. Goldman, Climbing, falling, and jamming during ant locomotion in confined environments. *Proceedings of the National Academy of Sciences* **110**, 9746-9751 (2013).
22. N. Gravish, G. Gold, A. Zangwill, M. A. D. Goodisman, D. I. Goldman, Glass-like dynamics in confined and congested ant traffic. *Soft Matter* **11**, 6552-6561 (2015).
23. D. Monaenkova *et al.*, Behavioral and mechanical determinants of collective subsurface nest excavation. *The Journal of experimental biology* **218**, 1295-1305 (2015).
24. P. Tenczar, C. C. Lutz, V. D. Rao, N. Goldenfeld, G. E. Robinson, Automated monitoring reveals extreme interindividual variation and plasticity in honeybee foraging activity levels. *Animal Behaviour* **95**, 41-48 (2014).
25. E. J. Robinson, O. Feinerman, N. R. Franks, Flexible task allocation and the organization of work in ants. *Proceedings. Biological sciences / The Royal Society* **276**, 4373-4380 (2009).
26. V. Fourcassie, A. Dussutour, J. L. Deneubourg, Ant traffic rules. *Journal of Experimental Biology* **213**, 2357-2363 (2010).
27. N. C. Darnton, L. Turner, S. Rojevsky, H. C. Berg, Dynamics of bacterial swarming. *Biophysical journal* **98**, 2082-2090 (2010).
28. A. John, A. Schadschneider, D. Chowdhury, K. Nishinari, Collective effects in traffic on bi-directional ant trails. *Journal of Theoretical Biology* **231**, 279-285 (2004).
29. C. R. Reid *et al.*, Army ants dynamically adjust living bridges in response to a cost–benefit trade-off. *Proceedings of the National Academy of Sciences* **112**, 15113-15118 (2015).
30. C. Gershenson, D. Helbing, When slower is faster. *Complexity* **21**, 9-15 (2015).
31. K. Nagel, M. Schreckenberg, A cellular automaton model for freeway traffic. *Journal de Physique I* **2**, 2221-2229 (1992).
32. R. Kuhne, in *Internation Symposium on Highway Capacity*. (1991).
33. M. J. Mataric, in *Proceedings of the Second International Conference on Simulation of Adaptive Behavior*. (1993), pp. 432-441.
34. M. J. Krieger, J.-B. Billeter, The call of duty: Self-organised task allocation in a population of up to twelve mobile robots. *Robotics and Autonomous Systems* **30**, 65-84 (2000).
35. S.-k. Yun, M. Schwager, D. Rus, in *Robotics Research*. (Springer, 2011), pp. 607-623.
36. K. N. Nordstrom, J. P. Gollub, D. J. Durian, Dynamical heterogeneity in soft-particle suspensions under shear. *Physical Review E* **84**, (2011).
37. Z. Jiang, Q. Kemao, H. Miao, J. Yang, L. Tang, Path-independent digital image correlation with high accuracy, speed and robustness. *Optics and Lasers in Engineering* **65**, 93-102 (2015).
38. D. I. Goldman, H. L. Swinney, Signatures of glass formation in a fluidized bed of hard spheres. *Physical review letters* **96**, 145702 (2006).
39. D. M. Gordon, The Evolution of the Algorithms for Collective Behavior. *Cell Systems* **3**, 514-520 (2016).
40. D. Jouvenaz, G. Allen, W. Banks, D. P. Wojcik, A survey for pathogens of fire ants, Solenopsis spp., in the southeastern United States. *Florida Entomologist*, 275-279 (1977).
41. MathWorks, Global Optimization Toolbox (R2016a). (2016).
42. N. Gravish, D. Monaenkova, M. A. D. Goodisman, D. I. Goldman, Climbing, falling, and jamming during ant locomotion in confined environments. *Proceedings of the National Academy of Sciences* **110**, 9746-9751 (2013).
43. V. Linevich, Master, Georgia Institute of Technology, (2015).

Supplementary Materials:

Materials and Methods, Videos

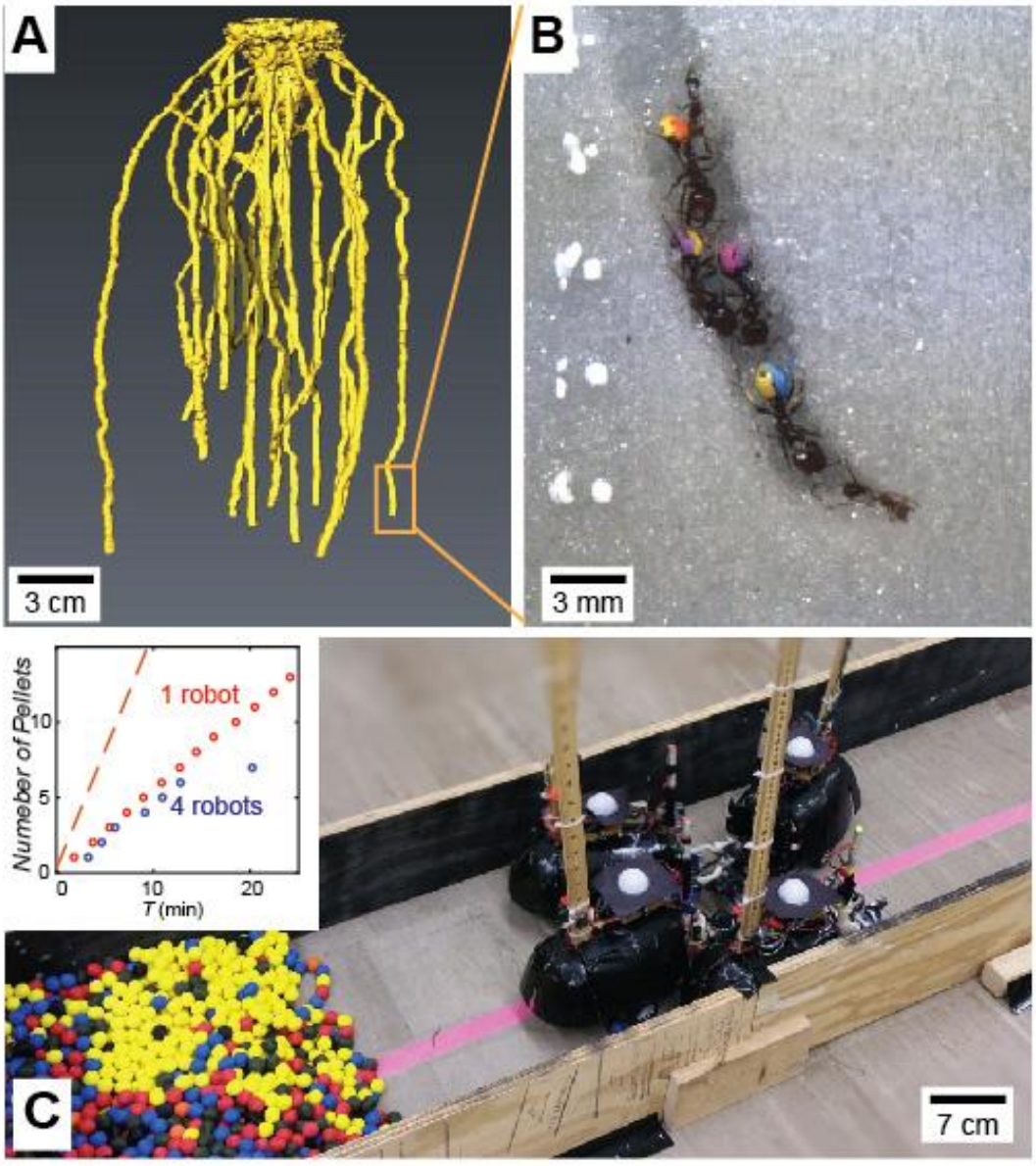

Fig. 1 Confined biological and robotic excavators. (A) X-ray reconstruction of *S. invicta* fire ant excavation in a container filled with 240-270 μm glass beads (B) Painted fire ants excavating a tunnel in 0.25 mm diameter wet glass particles. (C) Autonomous robotic diggers excavating in simulated environment with cohesive granular media (diameter 1.8 cm). (Inset) Number of pellets (defined as a cohesive group of grains) deposited vs time by a robot excavating alone (red dots), and the net excavation of four robots (blue circles), whereby each robot attempts to excavate maximally. Orange dashed line indicates the performance of the group of four robots in the absence of confinement.

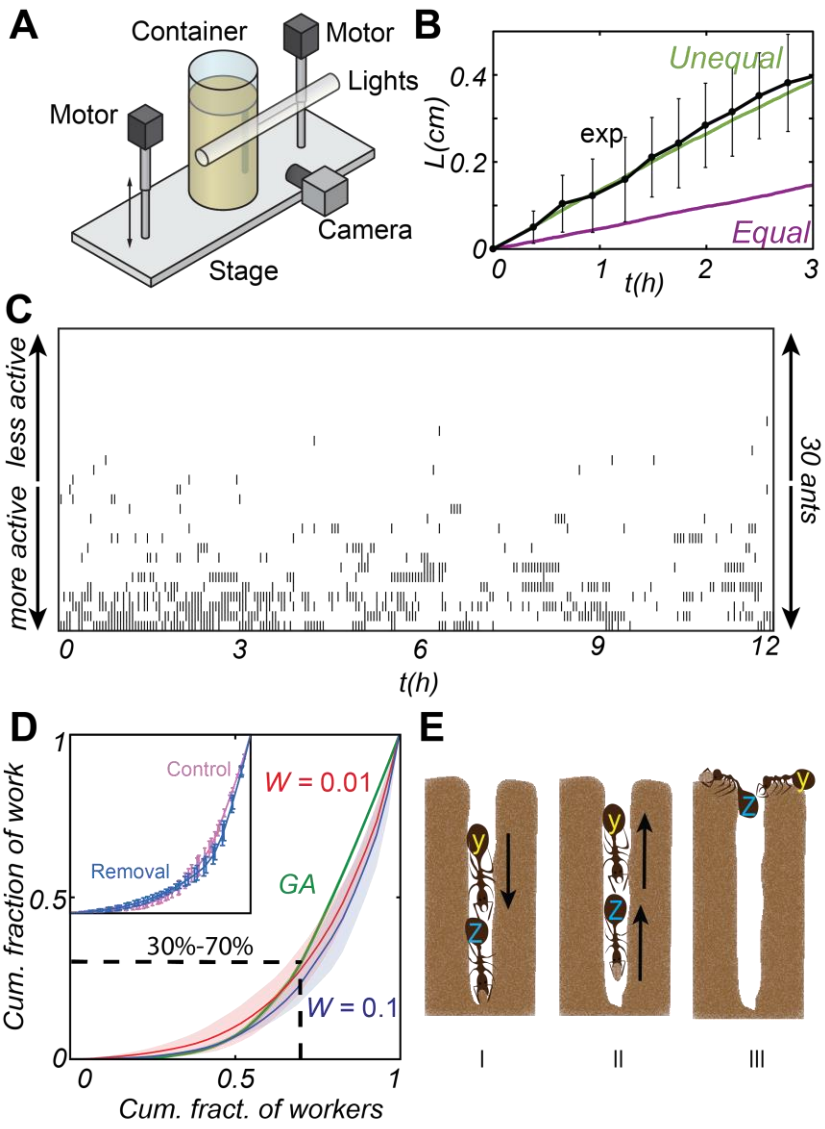

Fig. 2 Biological observations reveal both idle and reversal behavior in ants. (A) Experimental apparatus to track ant excavation; container inner diameter is 5.21cm. (B) The growth of tunnel length over time: experimental results (black) and simulations for groups with equal (purple) and unequal (green) workload distribution. Error bars denote 1 standard deviation in each direction. (C) "Visitation" map derived from experimental data. Each point in the map indicates the presence of a particular ant (out of 30 ants) ordered from most active to least active (y axis) in the tunnel at a time *t*. (D) Lorenz curves for workload distributions obtained in wet 0.25 mm diameter glass particles with moisture constant of $W = 0.1$ (blue) and $W = 0.01$ (red), and a CA-model (green) whose excavation rate was optimized with a genetic algorithm. Shaded areas correspond to standard deviation from 3 experiments. (Inset) Lorenz curves for a workload distribution within the group before (control, purple) and after (repeat, blue) the most active diggers are removed from the group. Error bars correspond to standard deviations from 3 experiments. (E) Illustration of observed reversal behavior. (I) Ant Y's path to excavate is blocked by ant Z. (II) When Z is finished collecting a pellet, it reverses, (III) forcing Y to reverse without excavating.

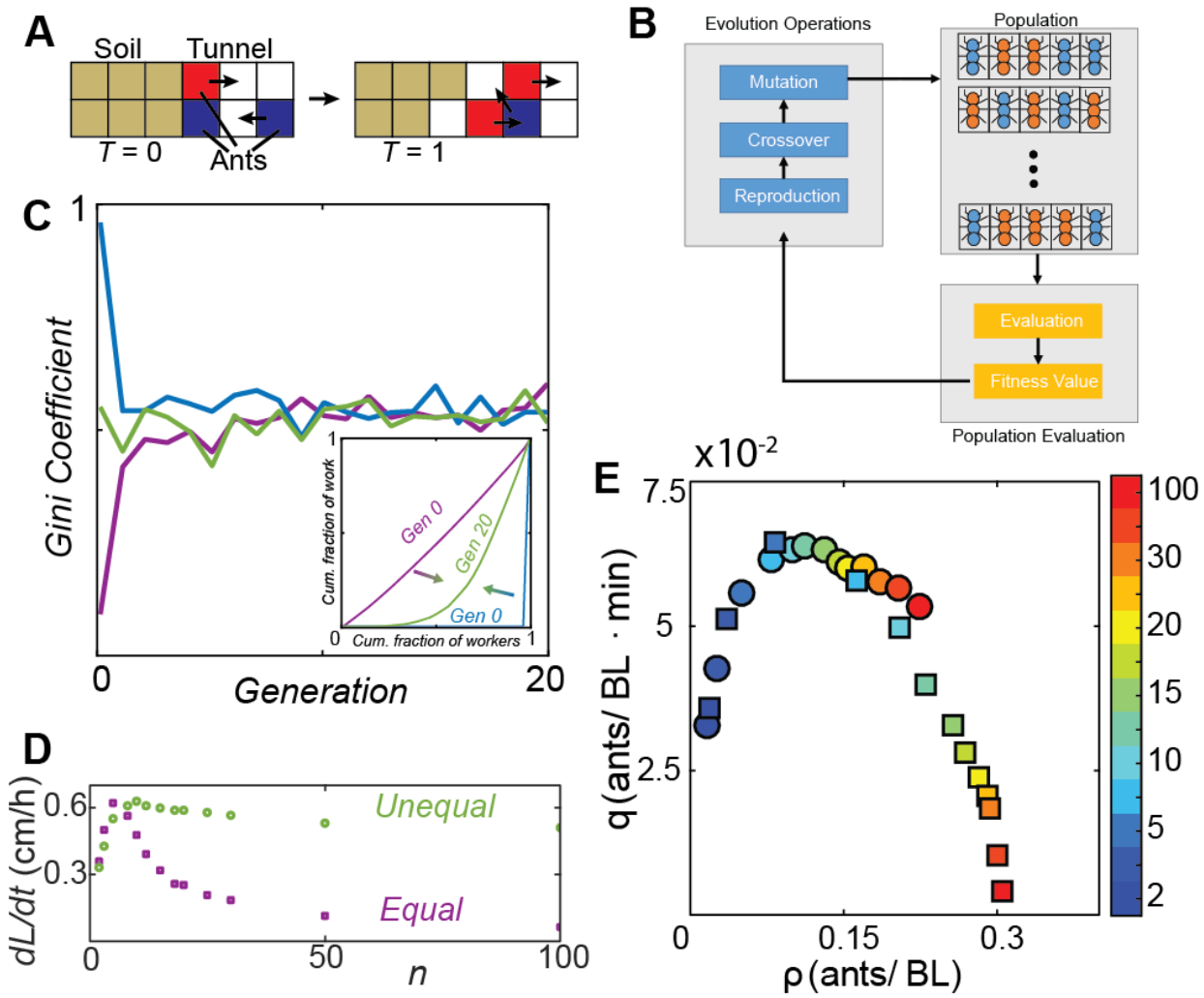

Fig. 3 Cellular automata simulations reveal benefits of unequal workload distribution in confined spaces. (A) Schematic, showing the main components of cellular automata model. Cell colors denote soil (brown), tunnel (white), ants moving towards the excavation site (blue) and exiting the tunnel (red). (B) Schematic of genetic algorithm, where each ant's (or "chromosome's") probability of entering the tunnel (or "gene") of a population represents an individual ant's probability to excavate. The groups with the highest digging rate of a generation are crossed over, and the least effective have a probability of mutation. (C) Gini coefficient vs generation for groups started with a completely equal (purple), completely unequal (blue) and random (green) workload distribution. Lorenz curves (inset) for groups that begin with complete equality or inequality rapidly reach a similar workload distribution. (D) Tunnel growth rate vs size of ant population for equally (purple squares) and unequally (green circles) active ants. Error bars are within the marker size. (E) Simulated traffic flow ($\bar{q}$) versus CA ant density ($\bar{\rho}$) for groups of equally (squares) and unequally (circles) active ants. Color bar indicates the size of the excavating group.

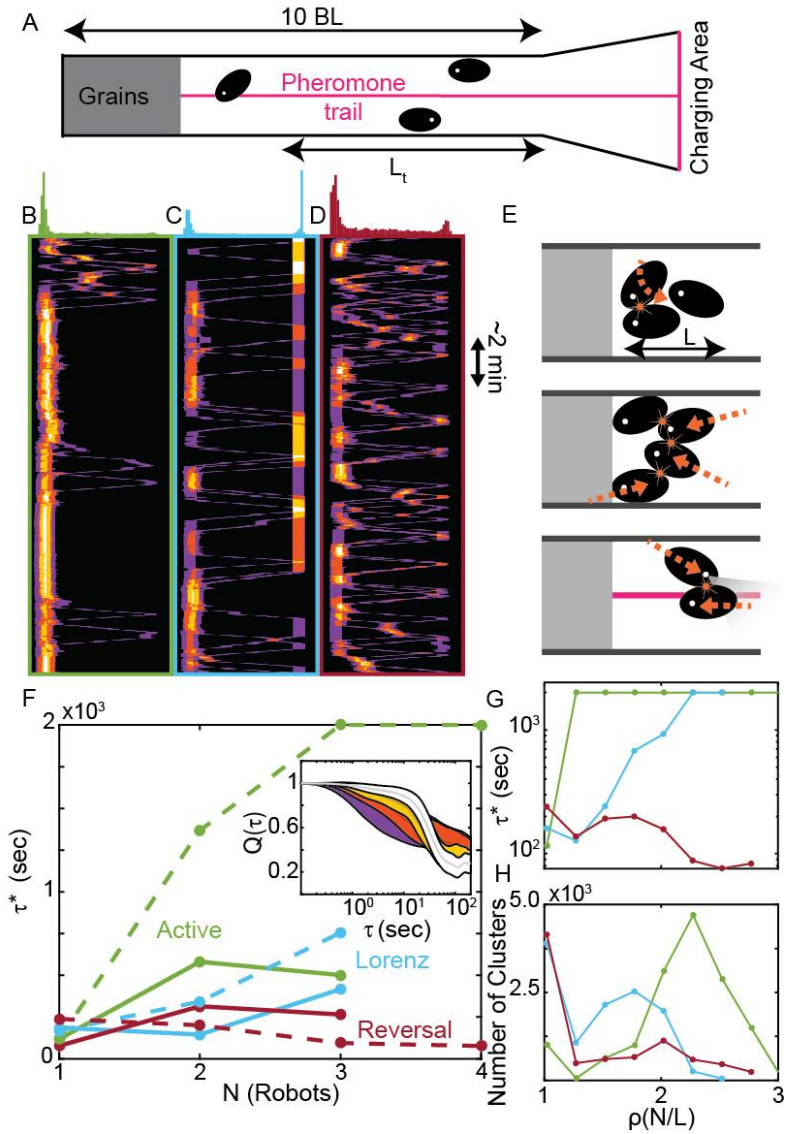

Fig. 4 Traffic flow and local dynamics during robot excavation. (A) Schematic of the excavation arena. A pink centerline along the tunnel was monitored by the robots' onboard cameras, enabling them to follow this emulated pheromone trail. (B-D) Experimental space-time overlap heat maps of robot positions (x-axis) for 4-robot trials of (B) Active digging, (C) Lorenz digging and (D) Reversal digging. Color indicates number of robots occupying a particular space and time from 1 (purple) to 4 (white) robots. Histograms on top of the graphs show the frequency of occurrence of clusters with 2 or more robots at different lateral positions. (E) Illustration of various collision scenarios encountered by robots due to turning (left), forward-backward translation (middle) and movement toward simulated pheromone trail (right). (F-H) Relaxation times for Active (green), Lorenz (light blue) and Reversal (maroon) strategies. (F) Relaxation time vs aggregation size for 3-robot (solid) and 4-robot (dashed) trials. (Inset) Sample average correlation curves, Q(τ), measure how 1 (purple), 2 (orange), 3 (yellow) and 4 (white) robot aggregations dissolve over time during 4-robot Reversal trials; shaded region indicates 1/2 standard deviation above and below average curves. (G) Relaxation times vs density for 4-robot trials and (H) corresponding number of aggregation occurrences vs aggregation density.

Supplementary Materials for

Idle active matter: excavation by confined and crowded collectives

D. Monaenkova[1], J. Aguilar[2], V. Linevich[2], W. Savoie[1], B. Dutta[1], M. A. D. Goodisman[3], and D. I. Goldman[1]*.

*Corresponding author. Email: daniel.goldman@physics.gatech.edu

This PDF file includes:

Materials and Methods
Supplementary Text
Figs. S1 to S13
Tables S1 to S2
References 39-43 (included in main reference list)
Captions for Movies S1 to S5

Other Supplementary Materials for this manuscript includes the following:

Movies S1 to S5

Materials and Methods

1. Ant Experiments

Ten *S. invicta* nests were collected during the spring, summer and autumn of 2014, 2015 and 2016 at the Research and Education Garden of the University of Georgia, GA, USA, and the Chattahoochee-Oconee National Forest, GA, USA. Nest collection and colony extraction were performed according to methods found in (*40*). Ants were housed in plastic bins for 2–3 months at an ambient room temperature of 23±3°C with a relative humidity of 30±2%, and fed Vespula larvae and supplied with tap water twice a week.

1.1 Primary Ant Digging Experiments

Small groups of 30 ant workers from the laboratory housed colonies were isolated in transparent containers filled with simulated cohesive soil made of 0.24 mm diameter wetted glass spheres (Ballotini glass beads). The experiments were conducted for 48 hours in W=0.01 and W =0.1 wet soils (3 trials for each soil moisture). All the experiments were repeated for 3 different colonies. The abdomens of the workers were marked in different colors. A plastic insert separated ants from cohesive soil and featured a single entry point next to the transparent wall of the container. A small (~ 5 mm) indentation was made next to the transparent wall of the container to prompt excavation. In all experiments, ants constructed a single tunnel. The top portion of the container was used by the ants for excavated soil deposition. The container was fixed on the motorized stage and the camera was focused on the first 2 cm of the tunnel, the distance approximately 4 ant body lengths. As the tunnel grew in length, the relative position of the tunnel and the camera were adjusted such that the tip of the tunnel was always visible. The camera was streamed, during which real-time processing detected the presence of ants based on pixel intensity. When an ant entered the camera's field of view, the camera was triggered to record 60 seconds of video, after which the software waited 2 minutes before searching for ants. The videos were analyzed to elucidate social behaviors that may affect excavation progress.

Work among excavators was characterized by counting the number of occurrences in which an ant visited the tunnel. Ants were classified as visitors if they appeared within the camera's view of the tunnel at any point within the duration of the experiment. Non-visitors were those ants that were never detected by the camera. Lorenz curves described the workload distribution by linking the cumulative share of visiting workers in the population (ranged from the least to the most hardworking individuals) to the cumulative share of work performed by the excavating group. The Gini coefficient (a measure of statistics dispersion) (*24*) derived from the shape of the curve reflected the inequality in the workload distribution within visiting group. In general, when the Gini coefficient is close to 0, the effort of the ants during the excavation is nearly equal. A Gini coefficient close to 1 indicates highly unequal workload distribution with a few active diggers in the visiting group carrying out the bulk of the workload. To calculate the Lorenz curves and Gini coefficients of the 48-hour experiments, the only ants that were included were those that were detected as having visited at least once during those 48 hours. To calculate the Lorenz curves and Gini coefficients for 12-hour epochs within those 48-hour experiments, we only considered the ants that visited within those 12-hour time-frames. This ensured that the calculated workload distributions only ever considered the working population of that measured time-period. Note that visitors which did not successfully dig and reversed without a pellet were also counted in the excavation effort; we argue that non-excavating visitors still expend energy in an excavation attempt and contribute to tunnel traffic. The first experiments revealed no significant effects of soil wetness W (1-way ANOVA, $F_{1, 12} = 0.78$, $P = 0.39$) on the Gini coefficients obtained from Lorenz curves built for the first 12 hours of tunnel construction.

1.2 Active Removal Ant Experiment

To determine how the removal of top 5 most active diggers from the colony affects the workload distribution and efficiency of tunnel construction, groups of 30 ants were set to excavate cohesive granular media. The excavation process was recorded for 3 hours. The ants were removed from the container and set to rest for at least 12 hours. The recorded data was analyzed to determine the 5 excavators that most contributed to tunnel construction. These active excavators were removed from the group and the experiment was repeated for an additional 3 hours. The rates of tunnel construction and the Gini coefficients were measured and compared for the first and the second parts of the experiment. The results were obtained in the experiments with three different colonies and averaged. Tunnel construction rates varied little between the two phases of the experiment. In fact, the growth rate increased slightly: 0.58 ±0.2 mm/ant within the first part of the experiment versus 0.67±0.3 mm/ant in the second part. The workload distribution also did not change and the Gini coefficient was 0.64±0.02 for control (first phase of experiment) and 0.61±0.02 for active removal (second phase). After the most active excavators from the first part were removed, several idle diggers increased their contribution to the excavation task. The contribution of the most active excavators within the first and the second parts of the experiment was comparable: 74±21% versus 74±5% of all observations in the tunnel. The most active diggers of the second part of the experiment had contributed to only 10±11.4% of total observations (546±65.8) during the first part of the experiment. Thus, individual ants were able to modify their behavior in response to the changing traffic dynamics of the tunnel.

2. Cellular automata model

We used a cellular automata model to elucidate the effects of sociality on traffic during tunnel construction. In a rectangular tunnel lattice, each cell could take one of four possible states: soil, sand, ascending excavator, and descending excavator. The initial conditions of the simulation included the number (n) of ants excavating in a group, ant size (s), the width of the tunnel (w), and the initial length of the tunnel as well as the protocol of social organization of the group. At every simulation step the ant was characterized by its 2D position (x,y), the direction of motion, whether or not they were carrying a pellet, and probability P to return back to the tunnel after pellet deposition.

The state of the cells in the model changed by a discrete time step according to a simple set of rules. At each iteration step, a CA ant located in the tunnel moved forward ("walked"), unless the cell in front of it was occupied by another CA ant. In this case, the ant moved to the cell adjacent to the occupied cell with probability p. This probability affected the duration of ant clusters and was chosen from the experimental data (as in (*22*)). Also, when in a cluster, a descending ant had a small probability to turn back and exit the tunnel without excavation ("reversal"). When the ant reached the tip of the tunnel, she spent several time steps excavating. The excavated pellet was transported to the tip of the tunnel and expelled from the tunnel ("pellet deposition"). After a predefined number of pellets were collected the tunnel grew in length by 1 cell. After pellet deposition the ant would return to the tunnel with probability P or switched to resting mode. In this mode, the ant was neither contributing to the excavation, able to cause clogs, nor increasing tunnel density. The exit from the resting mode was also defined by probability P.

Due to the geometrical constraints of the CA model, the reversal behavior was an essential to prevent jamming for infinitely long times for populations $n > 2 \cdot w/s$. In the absence of the

reversal behavior, an unresolvable jam consisting of $2 \cdot w/s$ ants formed and disrupted the excavation process. Thus, reversal behavior was implemented for all CA simulations regardless of workload distribution.

The unequal workload distribution was achieved by introducing the probability, *P*, to return to excavate in the tunnel after a pellet deposition. To simulate fully active ants, workers returned to the tunnel immediately after pellet deposition ($P = 1$). In groups with unequal workload distributions, the probability of the ant to return to the tunnel was unique, fixed and derived from the experimental ant workload distribution measurements as $P(\frac{n_i}{n}) = f\left(\frac{n_i}{n}\right) - f(\frac{n_i - 1}{n})$, where n_i was the number of ant in a sequence from the least to the most active; *n* was the excavating group size, and f was a Lorenz power law function.

TABLE S1

Dt	**0.5 s**
Ant size	**1 cell**
Tunnel width (w)	**2**
Reversal probability (P)	**0.34**
Sim length	**345600 steps (48 hrs)**
dt to drop pellet	**20**
Probability to move sideways (p)	**0.52**
Probability to move forwards	**1**
Excavations to grow tunnel size by 1 cell	**200 steps**

All parameters in the simulations were chosen such that the simulated tunnel growth rates for the last scenario would match the tunnel growth rates observed experimentally. The rates were calculated from the slope of the tangential lines fitting the initial portion of the tunnel growth curve. The tunnel excavation rates in simulations differed greatly depending on excavation scenario. In general, the groups of active diggers ($P = 1$) were most efficient when the number of excavators in the group was small. The increase in the number of active excavators led to the formation of ant clusters, which eventually slowed the nest construction down. The unequal workload distribution $P(\frac{n_i}{n})$ in the large groups of excavators allowed for reduction of ants density in the tunnel throughout the experiment and, thus, produced high nest construction rates even when the number of diggers in the excavating group was large. In large groups of diggers with unequal workload distributions, the excavation rates were largely insensitive to the addition of excavators.

2.1 Density and flow in CA model

The CA simulations were carried out for ant groups of different sizes. The ant density and the flux were measured in L = 8 cell long tunnel (~4 cm actual length). The flux and density were measured at $i = L/2+1$ position in the simulated tunnel (Fig. S5). Similarly to (*31*) we have introduced ant density as:

$$\bar{\rho} = \frac{1}{T}\sum_{t=1}^{T} n_i(t) \qquad (1)$$

where $n_i(t) = 1$ if the site is occupied at time t and 0 otherwise. Density at a fixed site i was averaged over a time period T=25 minutes. The average bi-directional flux $\bar{q}^T$ between site i and neighboring sites $i + 1$ and $i - 1$ was defined as

$$\bar{q} = \frac{1}{T}\sum_{t=1}^{T}\left[n_{i,i+1}(t) + n_{i,i-1}(t)\right] \quad (2)$$

where $n_{i,i+1}(t) = 1$, if the ant moved between sites i and $i+1$ and $n_{i,i-1}(t) = 1$ if the motion occurred between i and $i-1$ and zero is the motion was not detected. The flux was averaged over time T corresponding to 25 minutes of experiment.

We introduced these definitions to compare traffic in groups of different sizes governed both equal and unequal workload distributions. The fundamental flow diagrams (tunnel flow $\bar{q}$ vs density $\overline{\rho}$) each experimental condition are provided in the main text.

2.2 Clustering characterization in CA model

The implementation of unequal workload distribution reduces the immediate density of the ants in the tunnel in simulations. As a result, the number of jams (N_j), their spatial (c_n) and time duration (T_j), as well as the number of ants involved in the jams j_n decrease, allowing for stable traffic formation (Fig. S6).

To analyze traffic, the jam was defined as agglomerations of 3 and more ants located in the neighboring cells at a simulation step *k*. The number of jams was defined as the total number of agglomerations observed over 50,000 simulation steps. Each simulation step was considered independently. The site occupancy time T_j was defined as the time it takes for a particular cell occupied by an ant involved in a jam to change its value from "occupied" to "vacant". The average spatial extension of the jam was defined as the number of cells occupied by the ants sequentially along the tunnel length. The number of ants involved in a jam, the cite occupancy time and the spatial extension of a jam were averaged over all simulation steps and results are reported on Fig. S6.

2.3 Optimal distributions CA using a genetic algorithm

A genetic algorithm (GA) was used to search for work probability distributions that produced optimal digging rates. The GA is a biologically inspired optimization technique used typically to find solutions where the parameter space is large. GAs modify or evolve populations of solutions at each generation, through processes known as reproduction and mutation, towards the optimal solution. Each probability distribution for a single simulation is known as a "chromosome", and each probability for a single ant are called "genes". The set of all chromosomes at each generation is called a population. The reproduction phase requires each chromosome to be run, and depending on the on the output of the objective function, the metric by which each chromosome is measured, certain chromosomes are selected to be parents for the next generation. Our implementation used the digging rate as the objective function. The best performing chromosomes, known as the elite percent go unchanged to the next generation. The rest of the chromosomes are paired up, and a percentage, known as crossover percentage, are crossed over. Crossover is where a random site is chosen along the length of a chromosome and the genes of the paired chromosomes are switched around that point. After crossover, all genes belonging to the non-elite group of chromosomes have

a chance, known as mutation probability, to be assigned a new random value, this helps to mitigate chances of becoming stuck in local minima (or maxima) of the optimized quantity.

We used MATLAB's genetic algorithm toolbox (*41*). Our selection type was the default used in MATLAB's GA toolbox, stochastic uniform. The specific values for our reproduction and mutation rates were as follows: we used 5% for the elite selection, 80% for the crossover fraction, and we subject a variable number to mutation according to an adaptable mutation rate, the default option for MATLAB. We used a population size of 200 probability distributions per generation, and ran 20 generations.

3. Robot Experiments

Groups of robots were set to operate in simulated environment. The environment consisted of a table top testbed, featuring a quasi 2D tunnel and a pellet deposit area. The pellet deposit area was also used to accommodate inactive robots. After pellet deposition each robot had a choice either to return to excavation immediately or to pause, which was defined by a corresponding social protocol. The tunnel was partially filled with a cohesive simulated media made of loose rare-earth magnets (BYKES Technologies) contained in 3D-printed plastic shells 1.8 cm in outer diameter. The width of the tunnel allowed for simultaneous side-by-side tunnel excavation by two robots. In our previous laboratory experiments (*42*), *S. invicta* constructed ~ 2 body length wide tunnels

3.1 Robot design

The design intent was to create an inexpensive yet functional robot which could be used as a tool to study the effect of social protocols on collective excavation in confined spaces. The design of the robotic workers implements readily available off-the shelf and open source parts. A list of major components is shown in Table 2 [below, adopted from appendix B (*43*)]. The reader is encouraged to see the master's thesis work of Vadim Linevich (*43*) for a complete list of parts and design schematics. Discussion of core components below provides insight into how robots work and what they are capable of.

TABLE S2.

Core components	**Purpose**
Pixy Camera	Navigation
Magnetometer	Navigation
Gyroscope	Navigation
DC gearmotors	Locomotion
IR Distance Sensors	Obstacle avoidance
Contact Switches	Collision detection
Servo Motors	Environment manipulation
Proximity Sensor	Simulated media feedback
Li-On Battery, Single cell	Power source
Voltage Sensor	Power management
Current Sensor	Power management
Arduino FIO	Data logging
Arduino DUE	Sensor I/O, robot control

Four identical robots were built.

3.2 Microprocessors

Each robot utilized an Arduino Due microcontroller to handle sensor I/O, computations, and logic. In summary, the microcontroller software was set up to have three user programmable behavioral modes described in the paper: Active (Fig. S7), Reversal (Fig. S8), and Lorenz (Fig. S9). Each item in the flow chart has various baseline control loops running responsible for obtaining sensor data, performing state estimation, and controlling the actuators.

An Arduino Fio microcontroller was also used to handle data logging. Current, voltage and the state of the behavior mode was recorded and stored on a micro SD card for future analysis.

3.3 Sensors

3.3.1 Navigation sensors

A low cost camera system (Pixy CMUcam5) was used to accomplish most of the navigation. The camera located the simulated pink pheromone trail and supplied the Arduino Due with centroid coordinates and the size of the detected pheromone trail object. A lane following algorithm was used to guide the robot between the excavation and the deposit sites.

A magnetometer further improved navigation. A robot could be pushed off course in the event of a collision with another robot and lose sight of a simulated pheromone trail. The magnetometer would be used to recover correct heading. A priori knowledge of the test bed layout was exploited and thus the robot knew in which direction it needs to orient itself to get towards a current goal. The magnetometer simulated the sense of gravity in animals

A magnetometer was also used in conjunction with a gyroscope to obtain turning feedback. The robot would change its turning strategy if it registered making no progress while attempting to turning around.

3.3.2 Collision sensors

Two short range (15cm) infrared sensors were used to detect objects and obstacles directly ahead. In the event of an obstacle detection, the robot would attempt to steer around. The robot could detect physical interactions with the other robots or the environment using mechanical switches embedded beneath a segmented robotic shell. Each shell segment rested on a mechanical switch which was triggered by physical contacts within the environment. Thus, not only the contact, but also its approximate direction was sensed.

3.3.3 Environment manipulation sensors

An infrared proximity sensor was mounted near the robotic gripper. The sensor was occluded in the event of a successful collection of model media making this event distinguishably recognizable. The same sensor was also used to trigger excavation behavior.

3.3.4 Power management sensors

A bidirectional current sensor, along with a battery voltage level sensor were used to monitor power consumption. The robot relied on these sensors to determine if it needs to get to the charging station and recharge its single cell 3.7V Li-On battery.

3.4 Actuators

The robot locomotion was enabled by a differential wheeled drive system. The robot could drive with speeds up to 18cm/s. Two servo motors were used to operate a robotic arm used for manipulation of the simulated granular media. One servo motor actuated a robotic gripper while the other motor could raise or lower the pitch of the arm.

3.5 Mechanical Design

Figure S10 below illustrates mechanical design. The robot's body was made with parts which were designed to be robust and are manufactured with a 3D printer. The design was modular, allowing easy access to and replacement of components. Most of the electronics (microcontrollers, power circuits, etc.) are safely hidden inside the robotic shell because the robots were expected to engage in many physical contacts.

3.6 Robot Tracking

The robots were tracked via an image intensity threshold routine (Fig. S11). For each experimental trial, an overhead camera recorded the tunnel area for about 30 minutes at 10 frames per second. For a given frame of video, the image was subtracted from an averaged background image. A threshold was then applied to identify pixels corresponding to the robots. Initial robot positions were manually approximated at the beginning of the video. The robot pixels were then divided into different regions using Voronoi cells generated with the initial robot position. The centroids of these regions were then used to recalculate the robot positions, which were subsequently used as approximations for the next frame.

3.7 Global Traffic Analysis

Excavation rate and energy expenditure where measured for excavation trials (3 trials of each experimental condition) of 2 to 4 robots and 3 different social protocols: Active, where all robots are programmed to enter the tunnel and excavate immediately after deposition, Reversal, where robots enter the tunnel upon deposition but also reverse to exit if path to excavation site is blocked for a predefined duration, and Lorenz, where there is an unequal probability distribution among robots to return to excavate after disposition. Lorenz ants were programmed to deposit after excavating and, once in the charging area, they returned to excavate according to their individual probability to return. If an ant robot did not immediately return to excavate they waited for some time before attempting to return.

3.8 Local cluster relaxation times

Tracking data was used to identify clusters of robots, defined as groups of robots whose center positions were within a robot length's proximity of each other. Robot lateral positions were represented as intensity potentials in a space-time intensity map, I (Fig. S13 A). Each robot was given a lateral intensity potential function (a half-cycle sine wave with one body length half-period was chosen) centered at the robot's lateral position. Clusters were identified as contiguous potentials. The local dynamics of these clusters were evaluated using a technique often used to study dynamic heterogeneities in non-biological active matter (*36*). At each time step, clusters were identified and evaluated using a correlation function derived from PIV cross-correlation techniques (*37*):

$$\boldsymbol{q(\tau)} = \frac{\sum_{x1}^{x2}(\boldsymbol{I(\tau,x)}-\bar{\boldsymbol{I}})(\boldsymbol{I(0,x)}-\bar{\boldsymbol{I}}_{\boldsymbol{0}})}{\sqrt{\sum_{x1}^{x2}(\boldsymbol{I(\tau,x)}-\bar{\boldsymbol{I}})^2 \sum_{x1}^{x2}(\boldsymbol{I(0,x)}-\bar{\boldsymbol{I}}_{\boldsymbol{0}})^2}}. \qquad (3)$$

The correlation overlap function, $Q(\tau) = \langle q(\tau) \rangle$ (where the brackets indicate a time average from time, $t = 0$ *to* τ, whereby t = 0 corresponds to the time step in which the cluster is identified), compares the spatial overlap of an aggregation (or cluster) at a specific time to the overlap of the aggregation's original lateral segment at a later time, τ (Fig. S13 B).

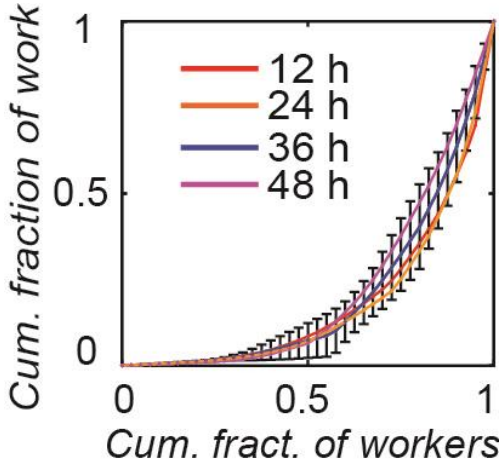

Fig. S1. Experimental Lorenz curves of ant workload distribution for individual 12-hour epochs of 48-hour trials. Error bars indicate standard deviation from multiple trials averaged over 6 trials (3 trials in ~0.25 mm diameter glass particles at W=0.1 moisture content and 3 trials in W=0.01).

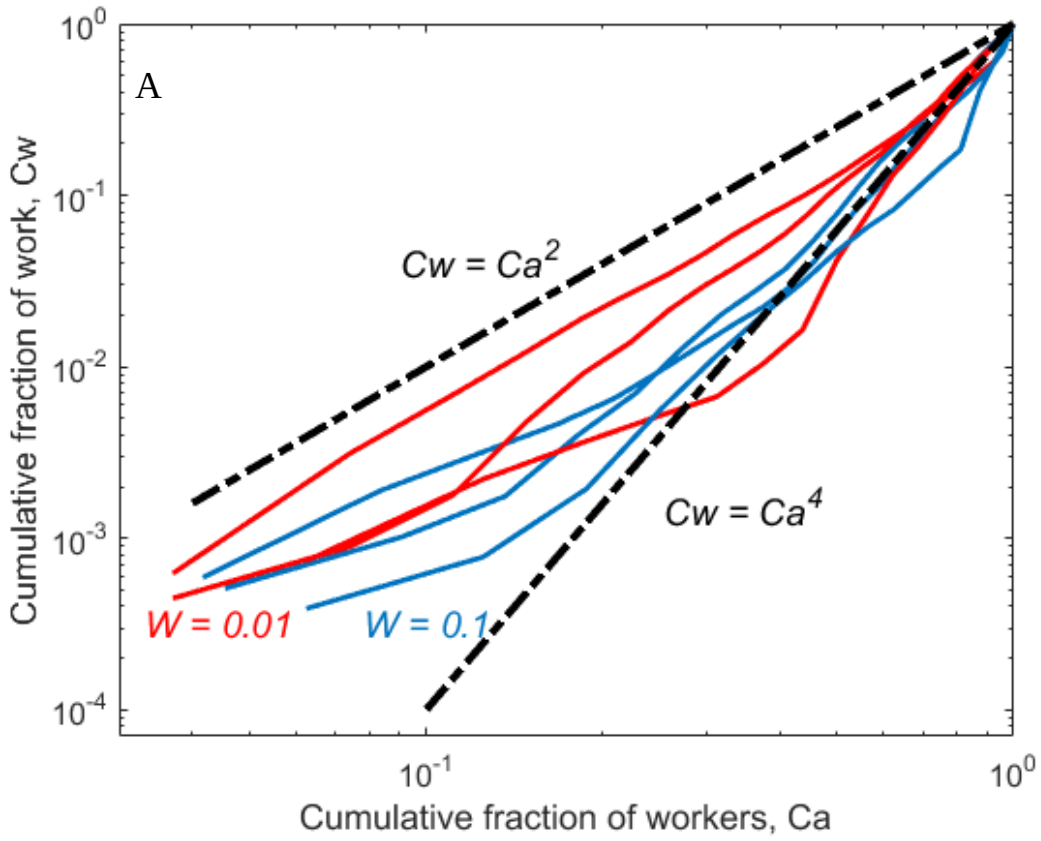
A
10^0
10^{-1}
10^{-2}
10^{-3}
10^{-4}
Cumulative fraction of work, Cw
$Cw = Ca^2$
$Cw = Ca^4$
$W = 0.01$
$W = 0.1$
10^{-1}
10^0
Cumulative fraction of workers, Ca

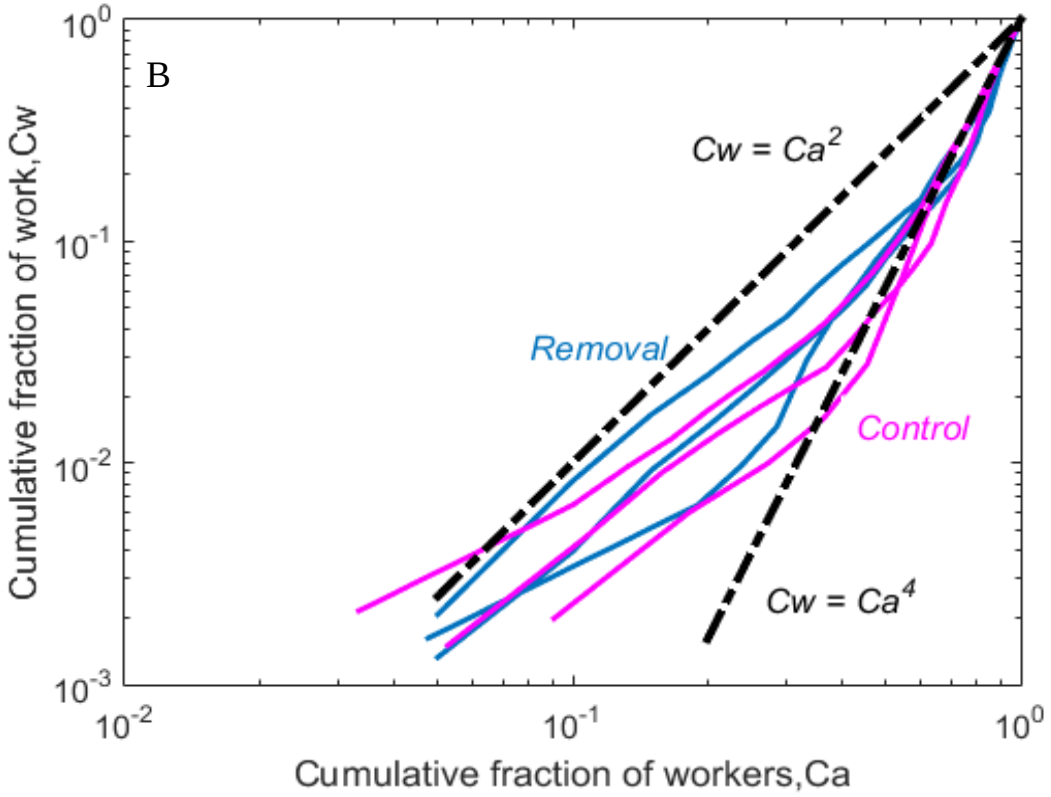

Fig. S2. Log-Log plots of Lorenz curves representing workload distributions in ant experiments (A) for different moisture contents and (B) for active removal experiment. Black dashed lines are power-law curves.

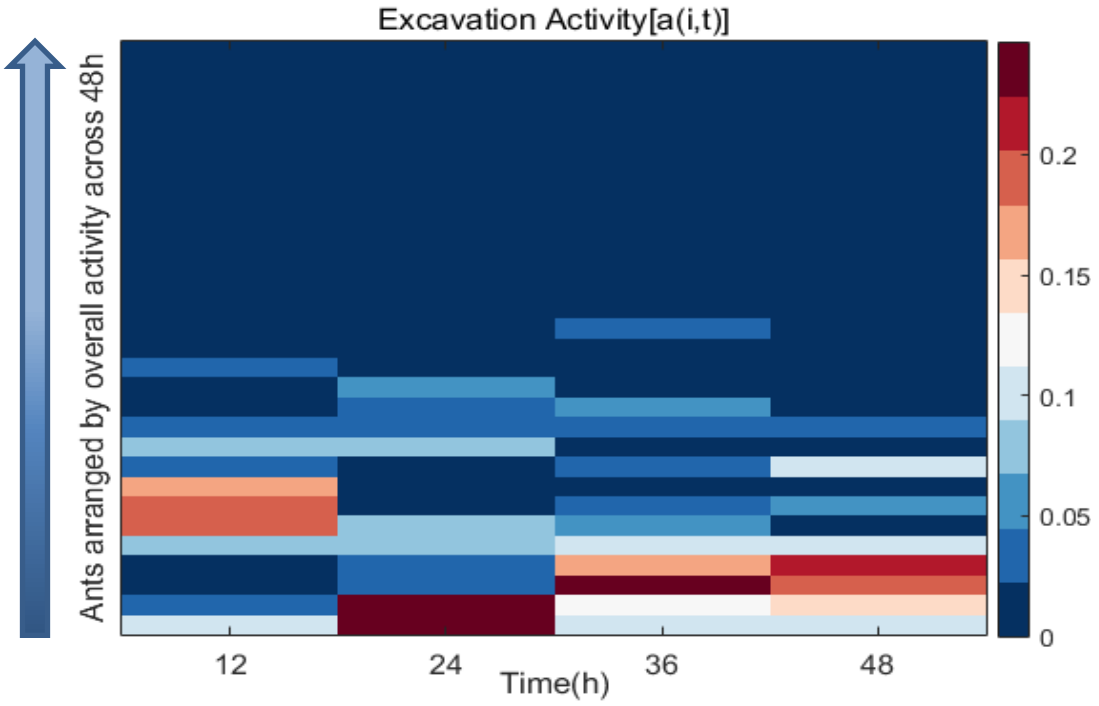

Fig. S3. Dynamic activity pattern of individual ants over different time epochs. The ants are arranged by their overall activity for 48-hours descending from bottom upwards. Excavation activity, **a(i,t)** is the number of tunnel visits per 12-hour epochs for an ant **i** divided by the total number of tunnel visits within that epoch.

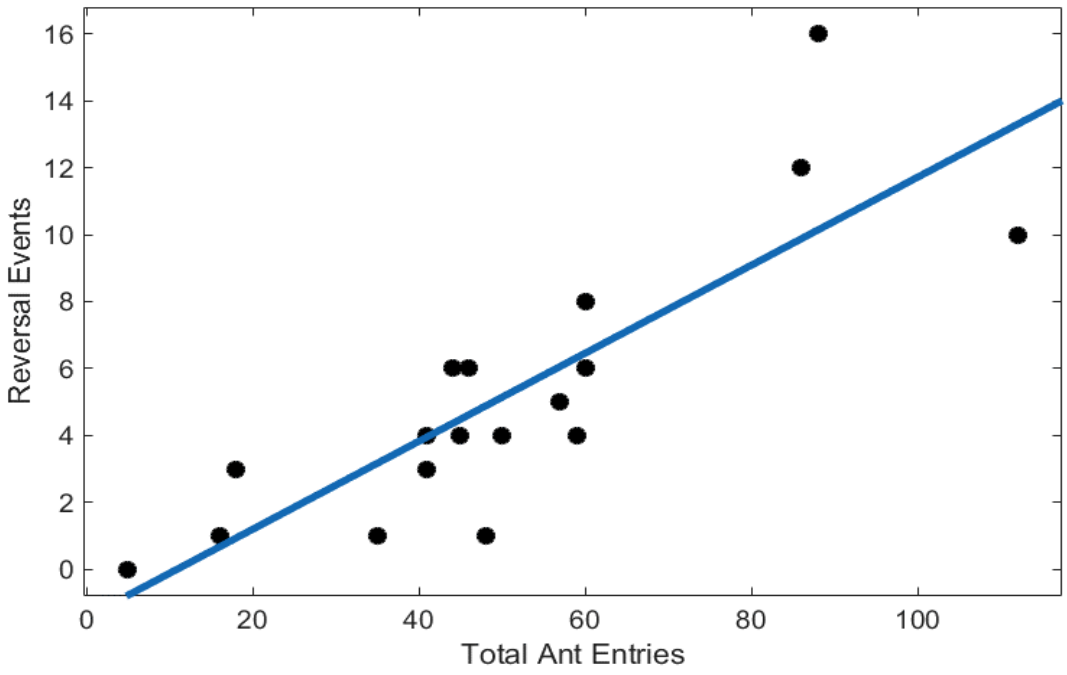

Fig. S4. Total number of reversal events vs total ant activity for first 3 hours of ant excavation. Each data point represents total reversal events and total entries counted for those 30 min segments. Data collected from 3 experiments. Linear fit (blue line) with R-squared of 0.69 repeated across 3 experiments for 10% moisture content

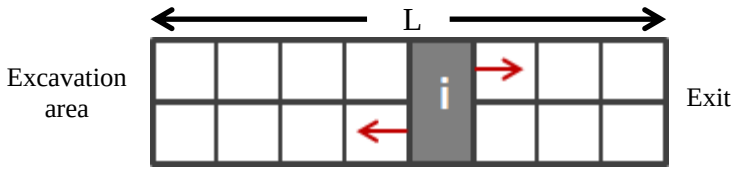

Fig. S5. Schematic of the tunnel in CA model. The density of ants and the flux in the tunnel were measured at the highlighted cell i. The possible directions of ant motion are shown with red arrows.

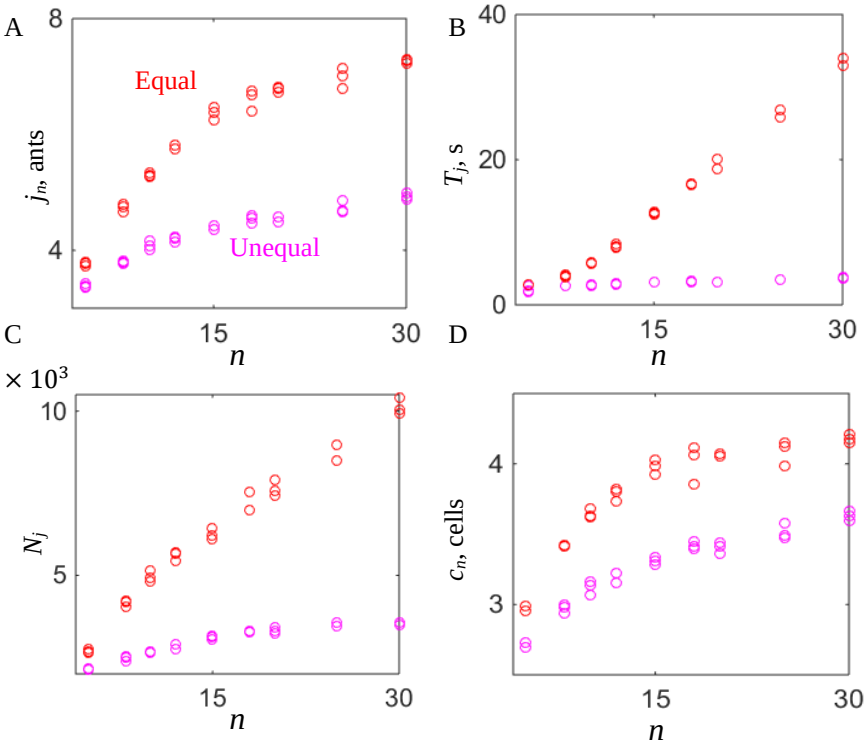

Fig. S6. Simulation results: Average number of ants involved in a jam j_n (A), site occupancy time T_j (B), total number of jams N_j over 50000 simulation steps (C) and average spatial extension of the jam c_n (D) plotted versus the size of the group for groups governed by equal workload distribution (red) and unequal workload distribution protocols (magenta).

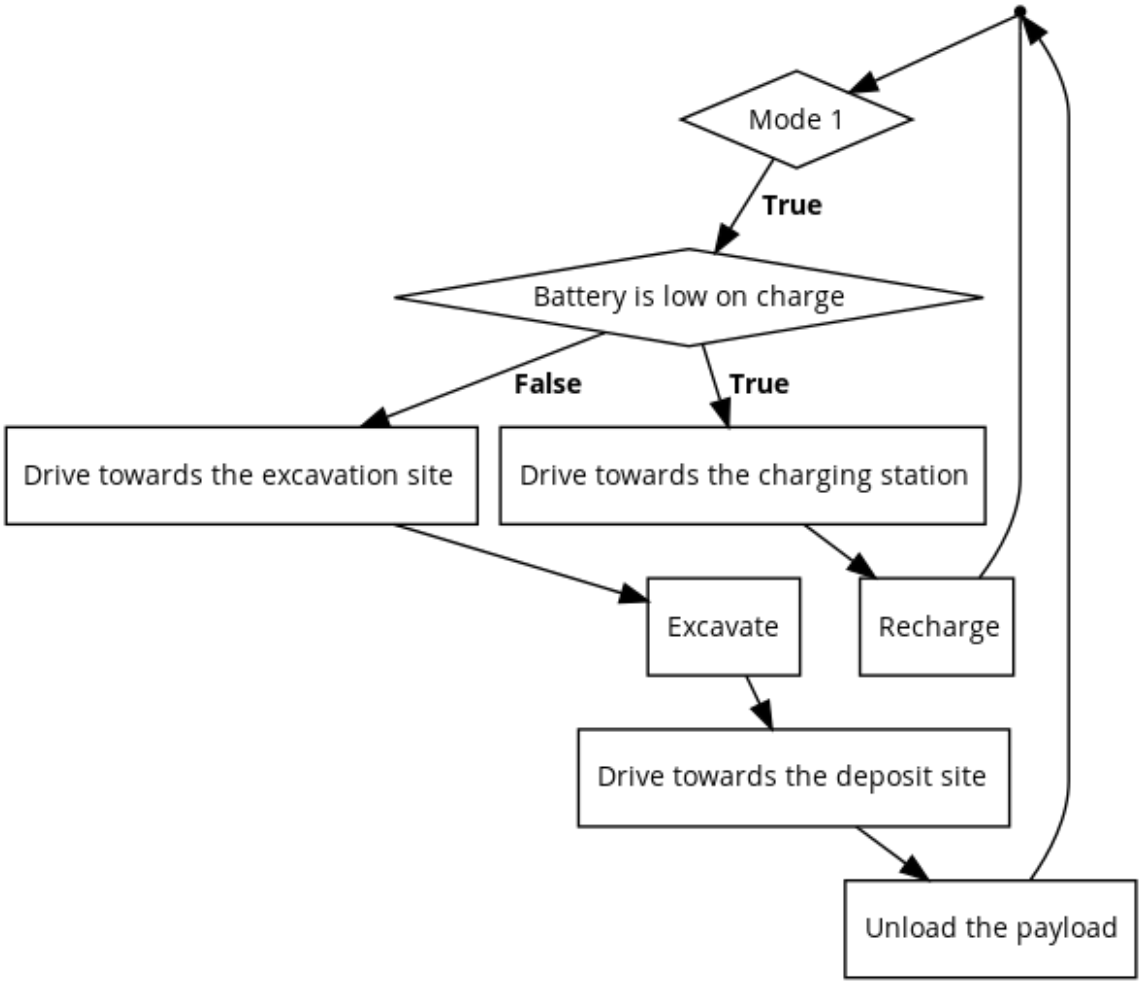

Fig. S7. Active (Mode 1) logic flow chart.

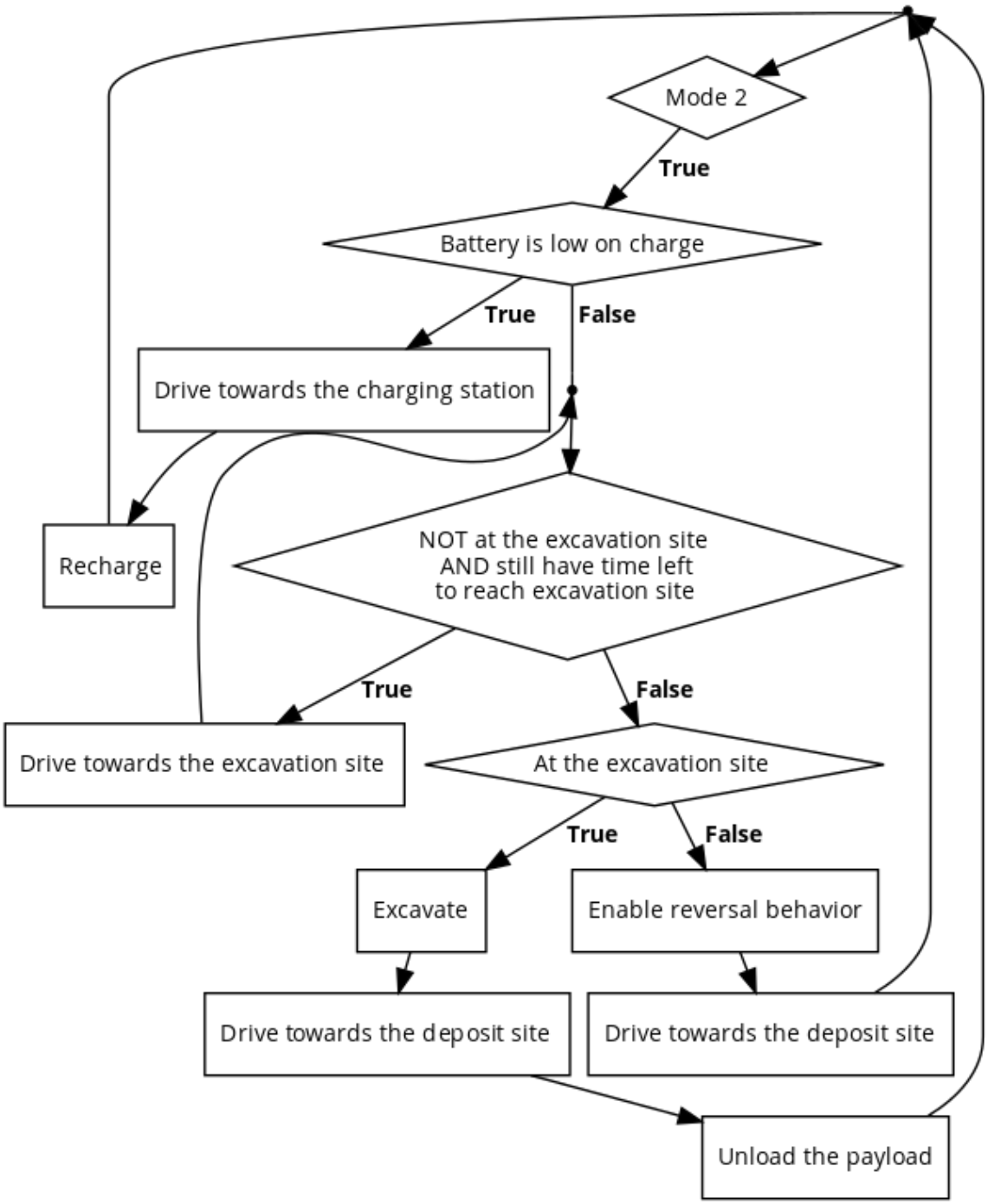

Fig. S8. Reversal (Mode 2) logic flow chart.

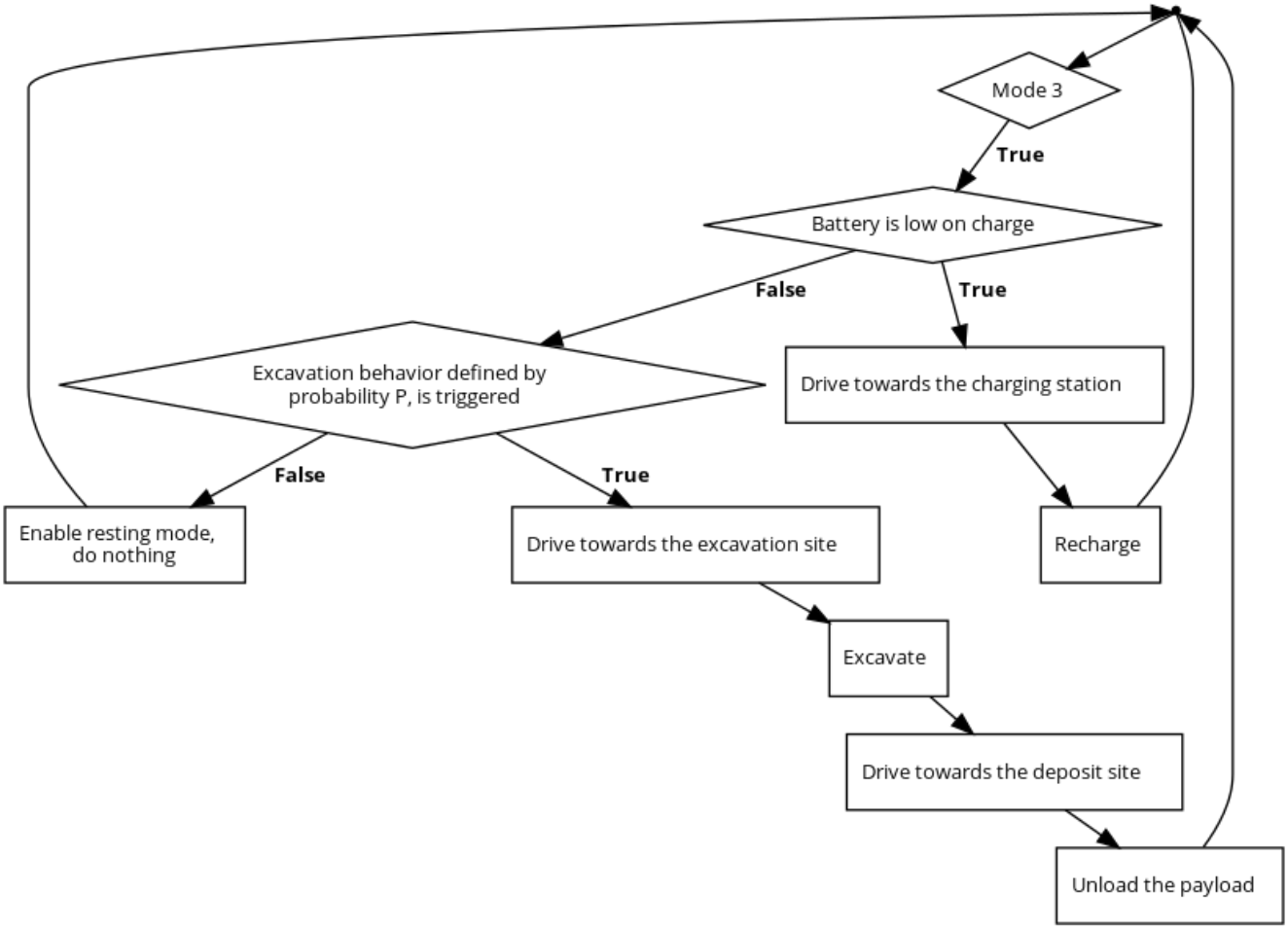

Fig. S9. Lorenz (Mode 3) logic flow chart. Note that this logic is identical to Active if P=1.

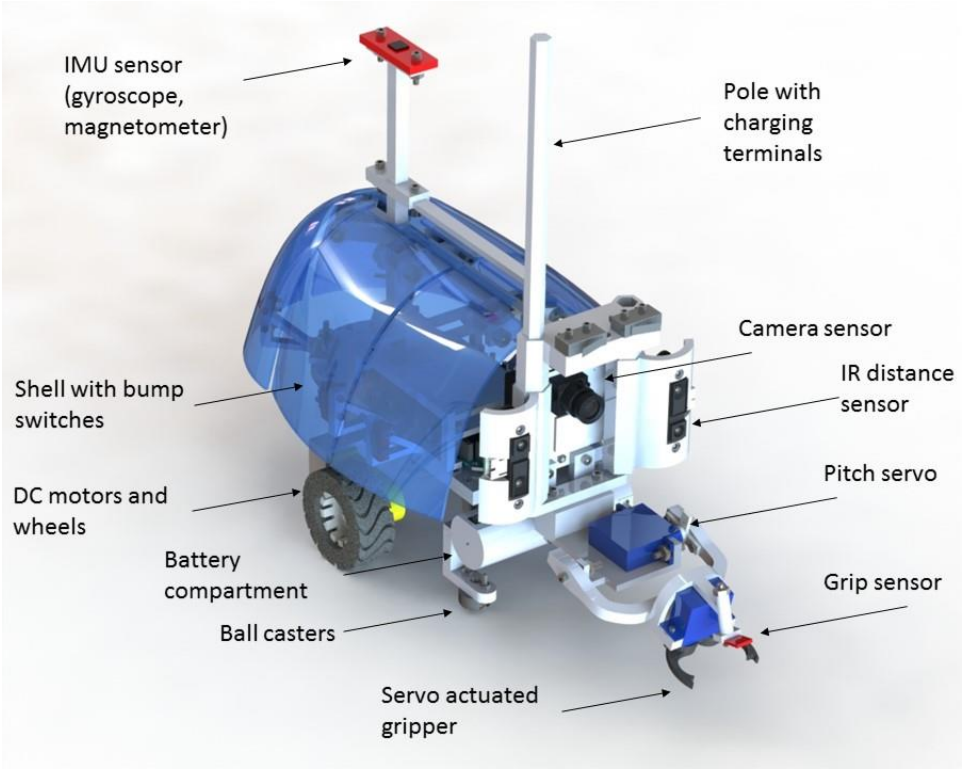

Fig. S10. Mechanical design. Microcontroller and circuitry are inside the shell

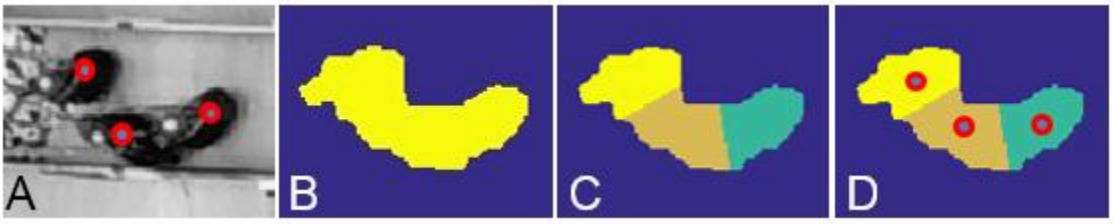

Fig. S11. Robot tracking routine. (A) Initial position estimates. (B) Threshold of background-subtracted image. (C) Voronoi divided robot regions. (D) Centroid calculated positions.

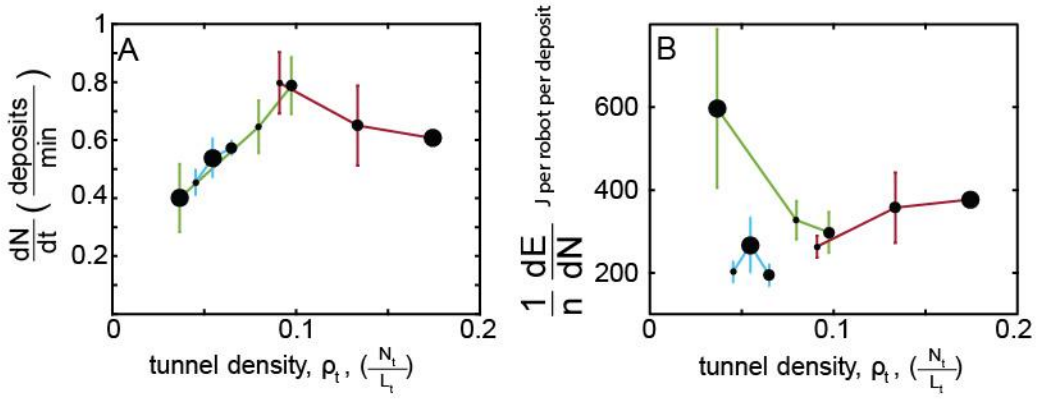

Fig. S12. Robot performance for 2 (smallest marker) to 4 (largest marker) robots using the Active (green), Reversal (maroon) or Lorenz (light blue) social protocol. (A) Fundamental diagram; excavation rate vs tunnel density, where N_t is the number of robots in the tunnel area and L_t is the length of the tunnel area in robot body lengths. (B) Energy expenditure vs tunnel density.

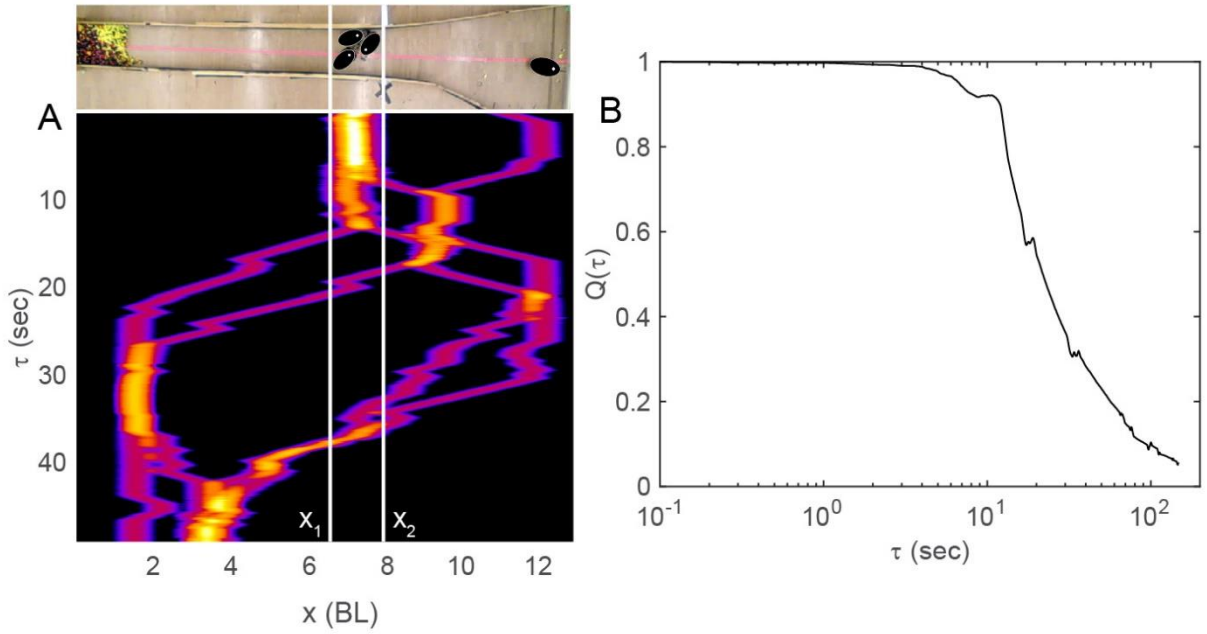

Fig. S13. Analysis of local robot clusters. (A) Sample space-time intensity map. (B) The correlation function Q(t) is calculated from the 3 robot cluster in the first frame in (A) (top panel).

Movie S1
Ant Activity experiments: Video of an ant (yellow-orange) giving up/reversing when faced with heavy traffic in tunnel.
Movie S2
Ant Simulation**:** Video of Cellular Automata (CA) simulation of ants with Active protocol (equal workload distribution) vs. Lorenz protocol (unequal workload).
Movie S3
Ant Robot: Video of a robophysical excavator following a pink line (representative of pheromone trail) and excavating simulated granular media (plastic hollow shells filled with magnets).
Movie S4
Ant Robot: Video of robophysical excavators encountering and resolving a jam while excavating magnetically adhesive granular media.
Movie S5
Robot experiments – Comparing protocols**:** Video comparing Active (top), Reversal (middle) and Lorenz (bottom) protocols implemented on excavating robots. Each Active robot exhibited maximum levels of activity. Reversal robots had a small probability to abandon the excavation attempt if the excavation area could not be reached within pre-defined time interval. Each Lorenz robot was assigned a distinct probability to re-enter tunnel after excavation. The proportion of lazy and hardworking robots is similar to observations of ant behavior.